This paper is published as part of a *PCCP* theme issue series on biophysics and biophysical chemistry:

Molecular Mechanisms of the Photostability of Life

Guest Editors: Andrzej Sobolewski and Wolfgang Domcke

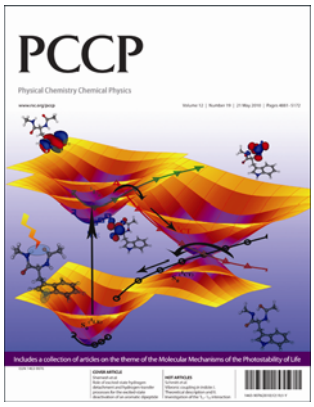

Editorial

Papers

The effect of C5 substitution on the photochemistry of uracil

Dana Nachtigallová,*[a] Hans Lischka,*[ab] Jaroslaw J. Szymczak,[b] Mario Barbatti,[b] Pavel Hobza,[a] Zsolt Gengeliczki,[c] Gustavo Pino,[d] Michael P. Callahan[e] and Mattanjah S. de Vries*[f]

Received 7th December 2009, Accepted 2nd March 2010
First published as an Advance Article on the web 27th March 2010
DOI: 10.1039/b925803p

A combined experimental and theoretical study on the excited-state behavior of the uracil analogues, 5-OH-Ura and 5-NH_2-Ura is reported. Two-photon ionization and IR/UV double-resonant spectra show that there is only one tautomer present for each with an excited state lifetime of 1.8 ns for 5-OH-Ura and 12.0 ns for 5-NH_2-Ura as determined from pump–probe experiments. The nature of the excited states of both species is investigated by means of multi-reference *ab initio* methods. Vertical excitation energies, excited state minima, minima on the crossing seam and reaction paths towards them are determined. Sizeable barriers on these paths are found that provide an explanation for the lifetimes of several nanoseconds observed in the experiment.

Introduction

Gas-phase and computational studies of RNA and DNA bases have revealed unique photophysical properties that are sensitive to subtle structural differences. Nucleobase excited-state lifetimes depend on isomerism,[1,2] substitution,[3,4] tautomer form[5,6] and non-covalent interactions, such as hydrogen bonding with complementary bases[7,8] or with solvent molecules[9] and stacking[10] bonding with other nucleobases. Theoretical understanding describes the excited-state dynamics in terms of rapid internal conversion mediated by conical intersections.[8,11–14] This pathway offers a mechanism to diffuse electronic excitation by converting it to ground-state internal energy which can be safely transferred to the environment. One intriguing implication is the possibility that this mechanism could have affected prebiotic chemistry on an early Earth, thus influencing the eventual make-up of the biomolecular building blocks that form life as we know it today.

Conical intersections that couple potential surfaces require geometrical changes in the excited states. For example for 9-methylguanine the internal conversion pathway seems to involve a strongly bent amino group at position 2.[15–17] The pathway for cytosine appears to involve C=C twisting[18,19] with a low barrier for keto-cytosine (producing a short vibronic spectrum[20]) and a considerable energy gap to the S_0 state for enol-cytosine, producing an extensive vibronic spectrum.[20] Therefore it should be no surprise that the potential energy landscapes that form conical intersections are affected by different substitutions. Excited-state dynamics should be especially sensitive to substitutions in the positions of the molecular frame that include coordinates along which the intersections are formed.

Among several works dealing with the effect of substitution in photoexcited nucleobases[4,14,21–28] we would like to draw attention to the recent work by Mburu and Matsika.[4] These authors have explored the effect of substitutions on purines and found that substitution at the C2 position decreases the energy of the first $\pi\pi^*$ state considerably whereas substitution at the C6 position has a much smaller effect; the carbonyl group has in general a stronger effect than the amino group; $n\pi^*$ states for all substituted purines are blue-shifted compared to purine. To understand the effect on pyrimidine bases they compared with 2-pyrimidinone (the ring structure of cytosine without the amino group) and found that the energy of the first bright excited state correlates strongly with the nature, position, and orientation of the substituent.

We have also recently explored the effect of amino substitutions in pyrimidines by studying 2,4-diaminopyrimidine by means of multi-reference *ab initio* methods.[29] The calculations of stationary points in the ground and excited states, minima on the S_0/S_1 crossing seam and connecting reaction paths show that several paths with negligible barriers exist, allowing ultrafast radiationless deactivation if excited at energies slightly higher than the band origin. Even though the NH_2 group attached to the C2 position blocks the path to one of the lowest energy conical intersections, namely the one associated with ring puckering at C2, there are still other alternatives for almost barrierless access to conical intersections associated with deformations at the C5, C6, and N1 positions.

Substituted uracil compounds can be viewed as structural analogues of 2,4-diaminopyrimidine in which the C2 and C4 positions are substituted by oxygen rather than amino groups (see Fig. 1). We now report the effect of substitution at the C5

[a] *Institute of Organic Chemistry and Biochemistry, Flemingovo nám. 2, 166 10 Praha 6, Czech Republic. E-mail: dana.nachtigallova@uochb.cas.cz, hans.lischka@univie.ac.at*
[b] *Institute for Theoretical Chemistry, University of Vienna, Waehringerstrasse 17, A1090 Vienna, Austria*
[c] *Department of Chemistry, Stanford University, Stanford, CA 94305-5080, USA*
[d] *National University of Cordoba, Argentina*
[e] *NASA Goddard Space Flight Center, Greenbelt, MD 20771, USA*
[f] *Department of Chemistry and Biochemistry, University of California Santa Barbara, CA-93106-9510, USA. E-mail: devries@chem.ucsb.edu; Fax: (+1) 805-893-4120; Tel: (+1) 805-893-5921*

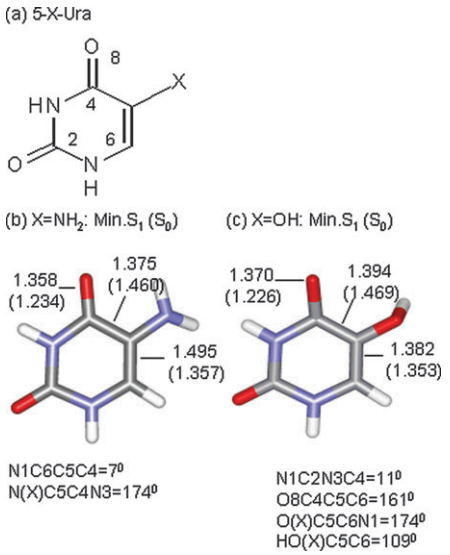

Fig. 1 (a) Structure and numbering of the 5-X-Ura molecule. Selected geometrical parameters of S_1 minima of (b) 5-NH_2-Ura and (c) 5-OH-Ura. Bond distances are given in Å. The ground-state parameters are given in parentheses.

position on excited-state relaxation of uracil analogues. We investigated two kinds of substitutions by experimental and computational methods, the OH substitution leading to 5-hydroxyuracil (5-OH-Ura) and the NH_2 substitution leading to 5-aminouracil (5-NH_2-Ura). Brady *et al.* have shown that 5-methyluracil (also known as thymine) has a broad UV spectrum at the band origin indicative of a short excited-state lifetime, similar to uracil itself.[30] But if the substituent is a hydroxyl or an amino group we found the excited-state lifetimes to be 1.8 ns and 12.0 ns respectively.

It appears that at the shorter wavelengths at which most of the time-dependent experiments have been conducted so far, all nucleobases are excited well above any possible barriers towards internal conversion. So to the extent that pathways through conical intersections exist, the photochemical behavior would be similar for all such species, and generally a short excited-state lifetime is observed in experiments at 267 nm.[24,31,32] On the other hand, our results show that the deactivation mechanisms following excitation to the origin of the first UV absorption band are very sensitive to the topography of the potential energy surface and thus lead to significant differences in excited-state dynamics of analogous species. This fact is especially relevant if we take into account that the intensity of the UV solar radiation in this range, about 300 nm, is most sensitive to the specific atmospheric composition.

Methods

Experimental methods

We laser desorb a mixture of pure compound from a graphite substrate with a Nd:YAG laser (1064 nm, ~10 ns pulse duration, less than 1 mJ/pulse), after which the molecules become entrained in a pulsed supersonic jet of Ar (backing pressure 6 atm). Using mass-selected spectroscopy we measure resonant two-photon ionization spectra (R2PI) by detecting positive ions in a reflectron time-of-flight mass spectrometer.[33] In UV-UV double resonance experiments, two laser pulses are separated in time by 200 ns. Ionization laser intensities are approximately 3 mJ/pulse and are attenuated to avoid saturation. The first pulse serves as a "burn" pulse, which removes ground-state population and causes depletion in the ion signal of the second "probe" pulse, provided both lasers are tuned to a resonance of the same isomer. In IR-UV double resonance spectra the burn laser operates in the near-IR region. IR frequencies ranging from 3100 cm^{-1} to 3800 cm^{-1} are produced in an optical parametric oscillator setup (LaserVision) pumped by a Nd:YAG laser operating at its fundamental frequency. Typical IR intensities in the burn region are 8–10 mJ/pulse with a bandwidth of 3 cm^{-1}. The resulting ion-dip spectra are ground-state IR spectra that are optically selected by means of the probe laser R2PI wavelength and mass selected by virtue of the mass spectrometer detection. We record excited-state lifetimes by following resonant excitation by ionization (290.3 nm for 5-OH-Ura and 312 nm for 5-NH_2-Ura) with a separate 266 nm laser pulse with variable delay.

Computational methods

To assign the IR-UV double resonance spectra, we calculated relative energies and vibrational frequencies of possible tautomers using the density functional theory (DFT) method employing the B3LYP hybrid functional[34–36] and a 6-311+G(2d,p) basis set.[37,38] To account for anharmonicity and method deficiency we scaled vibrational frequencies by a factor of 0.9618. We used the Gaussian 03 quantum code package.[39]

The minima on the ground and excited S_1 surfaces and on the S_1/S_0 seam of conical intersections (MXS) were determined by means of the complete active space self-consistent field (CASSCF) method. The active space for CASSCF wavefunctions was constructed by using ten electrons in eight orbitals (10, 8), which comprises one lone pair (n) located on the oxygen atom of C4-O carbonyl group and seven π orbitals. A state-averaging procedure including three states (SA-3) was used. The localization of the minima on the crossing seams were performed by means of the analytic gradients and nonadiabatic coupling vectors.[40–43] Multi-reference configuration interaction (MR-CI) and multi-reference second-order perturbation theory in its multi-state version (MS-CASPT2) method[44,45] were used to account for dynamic correlation effects. Unless specifically stated the 6-31G* basis set was used throughout the calculations.[46]

In the CI approach, single and double excitations from the CI reference space are included and the generalized interacting space restrictions are adopted.[47] The MR-CISD reference space was constructed by moving orbitals with natural occupation larger than 0.9 and smaller than 0.1 to the doubly occupied and virtual spaces, respectively, resulting in the space composed of six electrons in five orbitals (MR-CISD(6, 5)). All single and double excitations were allowed from this reference space. To reduce the computational cost during the geometry optimization, 14 doubly occupied orbitals were frozen. This procedure was tested against calculations with nine 1s core

orbitals frozen for a selected set of structures. The size-consistency effects were taken into account by means of the Pople correction method[40,48,49] and are indicated by +Q. MS-CASPT2 calculations were performed with the same reference CAS space and with an IPEA shift of 0.25.[50] To verify the reliability of the 6-31G* basis set we performed these calculations using the 6-311G* basis set also. Reaction paths between selected stationary points and MXS structures were constructed using the method of linear interpolation of internal coordinates (LIIC). For these calculations we have used the MR-CI with singles (MR-CIS) and CASPT2 methods. The calculated energies of individual points are plotted as a function of the mass-weighted distances between these points and a stationary point.

The geometry of the ground-state minima were obtained using the resolution-of-identity coupled cluster to the second order (RI-CC2)[51–53] method using the TZVPP basis set.[54a] The vertical excitation energies obtained using this method are also reported. Absorption spectra were simulated by sampling the molecular geometries of the ground state by a harmonic oscillator Wigner distribution and then computing the photo-absorption cross section[55] for two excited states at the RI-CC2 level with SVP basis set.[54b] Five hundred points were sampled in the Wigner distribution and a normalized Lorentzian line shape with 0.1 eV width was employed. The optimization of conical intersections was performed using the analytic gradient and non-adiabatic coupling vectors[40–43] available in the COLUMBUS program system.[56–58] The CASPT2 calculations were performed with the MOLCAS program package.[45,59] RI-CC2 calculations were performed using the Turbomole program package.[60] Spectra simulations were performed with the Newton-X program.[61,62]

Results and discussions

Before measuring excited-state lifetimes by pump–probe measurements, it is necessary to determine the tautomeric forms we observed in the beam. Therefore the experiments consisted of the following sequence of measurements: (1) Obtain the UV R2PI spectrum. (2) Determine the number of tautomers in the spectrum by UV-UV hole burning. (3) Obtain the IR-UV double resonant spectrum for each tautomer. (4) Identify the tautomeric form(s) by comparison with computed frequencies. (5) Perform pump–probe measurements to obtain excited state lifetimes. Figs. 2 and 3 show the results for steps (1)–(4) for 5-OH-Ura and 5-NH_2-Ura, respectively. The signal-to-noise ratio in the in the R2PI spectrum of 5-OH-Ura is much poorer than for 5-NH_2-Ura, which may explain the lack of discernable vibrational progression in the former. Based on the comparison of calculated vibrational frequencies for the six lowest energy tautomers with IR spectra of both species we can assign the spectra to only a single tautomer, which is the lowest energy form. As shown in Fig. 2 for 5-OH-Ura, all di-enol tautomers are absent because we do not observe any vibrations between 3500 and 3600 cm^{-1}. Structure D is absent because we observe three, rather than two peaks. Of the two lowest energy structures A and B we observe form A in which the OH is slightly hydrogen bonded and therefore red-shifted relative to the free frequency in B which would be close to 3700 cm^{-1}. This red-shift is very hard to predict accurately, explaining the relative discrepancy with the measured value. For 5-NH_2-Ura, all enol tautomers are absent because we do not observe any vibrations beyond 3500 cm^{-1} (not shown in the figure). The imino form, C, would have exhibited fewer peaks. The only reasonable assignment is therefore the lowest energy form, A. The asterisks in the R2PI spectrum mark all wavelengths at which we obtained double resonant spectra with all identical results, confirming that the UV spectrum is due to the single tautomer only.

Fig. 4 shows the pump–probe measurements, obtained by two-color ionization with a variable delay between excitation and ionization. We fitted the data with single exponential decay curves, yielding lifetimes of 1.8 ns for 5-OH-Ura and 12.0 ns for 5-NH_2-Ura.

To explain the nature of the excited states of both species we performed further modeling by means of multi-reference *ab initio* methods. Below we report the results of the investigation of the potential energy surface, *i.e.* energetics of the excited states at the Franck–Condon region, excited state minima and minima on the crossing seam. Based on their relative energies and on the character of reaction paths connecting these points we can provide an explanation for the long excited-state lifetimes we observed experimentally.

Excited-state analysis

Vertical excitation energies of 5-NH_2-Ura and 5-OH-Ura. The valence bond structure and numbering scheme of 5-NH_2-Ura and 5-OH-Ura analogues and their optimized structures are shown in Fig. 1. The vertical excitation energies of both compounds are collected in Table 1. The ground state of 5-OH-Ura is of C_s symmetry, while due to the nonplanarity of the NH_2 group it is of C_1 symmetry for 5-NH_2-Ura. To keep the interpretation of the results consistent we will use the notation of C_1 symmetry for the vertically excited states of both species. The vertical excitation energies of two first excited states were calculated at the RI-CC2, CASSCF(10,8), MR-CISD(6,5), and MS-CASPT2 levels (see Table 1). In Table 1 the oscillator strengths calculated at the RI-CC2 level are also reported.

At the CASSCF level the first excited state in the ground-state minimum is due to excitation from the lone pair orbital localized on the O atom of the C4–O group, followed by excitation from the π-orbital localized mainly on the C5–C6 bond into a π* orbital. The orbitals involved in the excitations are shown in Fig. 5 for the case of 5-OH-Ura. Similar orbitals are involved in the excitations of 5-NH_2-Ura. Inclusion of dynamic correlation effects in MS-CASPT2 calculations results in a significant change in excitation energies of the ππ* state with the energy lowering leading to a reverse ordering of states. Note that even at the MR-CISD(6, 5) level the excitation energies of the ππ* state are still high. With Pople corrections included, the ordering of the states becomes the same as at the CASPT2 and CC2 levels.

The energy ordering of the states in the Franck–Condon region of 5-NH_2-Ura and 5-OH-Ura is reversed compared to the natural bases uracil and thymine (5-CH_3-Ura). The CC2

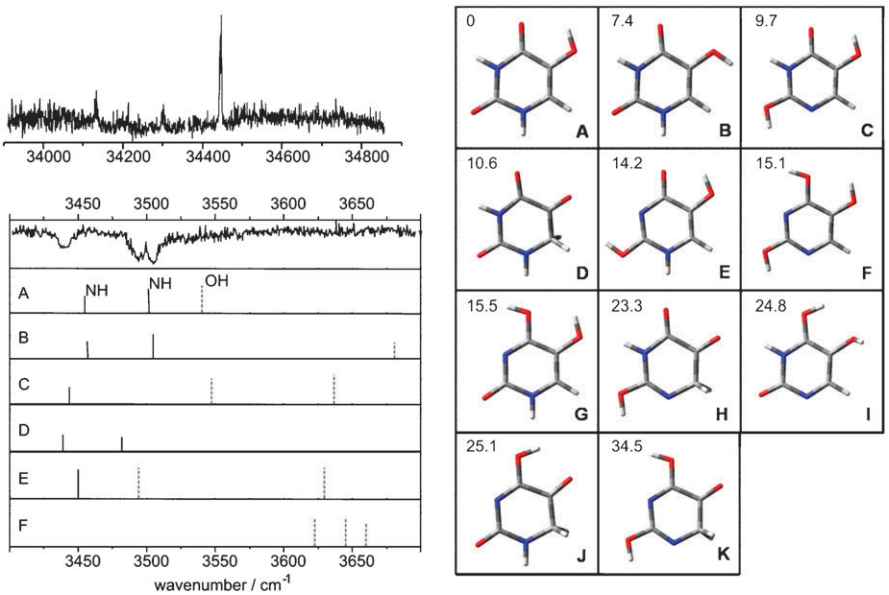

Fig. 2 Results for 5-OH-Ura. Top left: R2PI spectrum. Right panel: possible tautomeric forms with calculated relative energies in kcal mol^{-1}. Bottom left: IR-UV double resonant spectrum (top trace) compared with computed IR spectra (displayed as stick spectra, with NH stretches as solid lines and OH stretches as dashed lines) for selected tautomeric forms. Calculations were performed at the B3LYP/6-311 + G(2d,p) level.

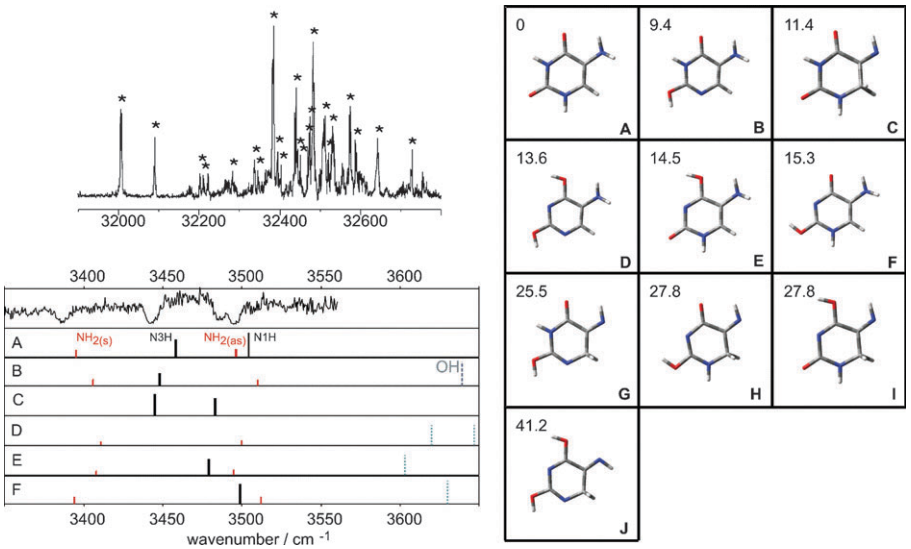

Fig. 3 Results for 5-NH_2-Ura. Top left: R2PI spectrum. Right panel: possible tautomeric forms with calculated relative energies in kcal mol^{-1}. Bottom left: IR-UV double resonant spectrum (top trace) compared with computed IR spectra (displayed as stick spectra with NH stretches as solid lines, OH stretches as dashed lines and NH_2 stretches as dotted lines) for selected tautomeric forms. Calculations were performed at the B3LYP/6-311 + G(2d,p) level.

method places the bright $\pi\pi^*$ state above the $n\pi^*$ state by about 0.6 and 0.4 eV for uracil and thymine, respectively (see Table 1). As will be discussed below, this inversion plays an important role in the dynamics of the uracil analogues.

In order to compare the experimentally measured vertical excitation energies with the values calculated using various methods described above we have simulated absorption spectra employing the RI-CC2/SVP method (see Fig. 6). The experimentally measured excitation energies at the band origin are 3.96 and 4.27 eV, for 5-NH_2-Ura and 5-OH-Ura, respectively. The energy difference between the band maxima and band origin estimated from the simulated spectra are 0.85 eV and 0.89 eV for 5-NH_2-Ura and 5-OH-Ura, respectively. Adding this shift to the experimental values of the band origin gives the energies of the band maxima of 4.81 eV and 5.16 eV for 5-NH_2-Ura and 5-OH-Ura, respectively. Compared to vertical excitation energies calculated with the CC2 method and the triple-ζ TZVPP basis set, which serve as benchmark calculations for vertical excitation energies, these values are 0.27 and 0.42 eV higher for 5-NH_2-Ura and 5-OH-Ura, respectively. The vertical excitation energies obtained at the CASPT2/6-31G* method are higher, with the energy difference within a small region of 0.2–0.3 eV compared to those obtained with the CC2/TZVPP method

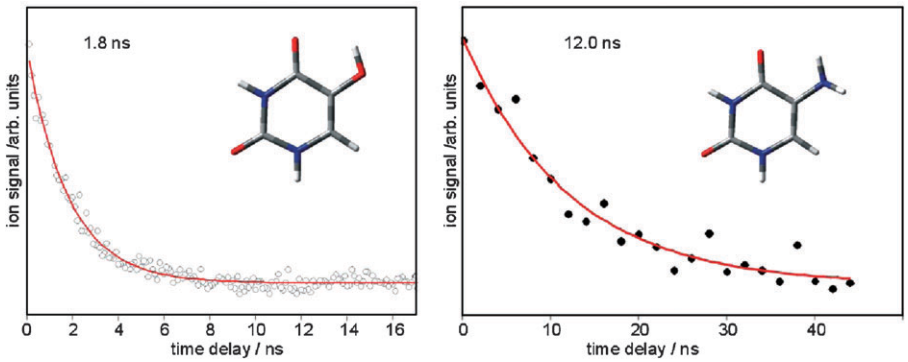

Fig. 4 Pump–probe data for 5-OH-Ura (left panel; pump: 290.3 nm, probe: 266 nm) and 5-NH_2-Ura (right panel; pump: 312 nm, probe: 266 nm). Solid line is a single exponential fit to the data.

Table 1 Vertical excitation energies and relative energies of min S_1 (in eV). Excited-state minima were optimized with 3-SA-CASSCF(10,8)/6-31G*, ground-state minima with RI-CC2/TZVPP

	Geometry	State	CASSCF(10,8)	MR-CISD(6,5)[a,b]	CASPT2[a,c]	RI-CC2[d]
5-NH_2-Ura	min S_0	$2^1A_1(\pi\pi^*)$	6.64	5.18 (5.98)	4.84 (4.69)	4.54 *4.82* (*0.185*)
		$3^1A_1(n\pi^*)$	5.12	5.49 (5.33)	5.21 (5.14)	5.06 *5.23* (*0.000*)
	min $S_1(n\pi^*)$	$S_1(n\pi^*)$	3.91	4.73 (4.18)	4.57 (4.54)	
		$S_2(\pi\pi^*)$	6.09	5.91 (6.56)	6.20 (6.15)	
5-OH-Ura	min S_0	$2^1A_1(\pi\pi^*)$	6.67	5.39 (6.18)	5.01 (4.96)	4.74 *5.07* (*0.189*)
		$3^1A_1(n\pi^*)$	5.25	5.69 (5.58)	5.37 (5.37)	5.20 *5.44* (*0.000*)
	min $S_1(n\pi^*)$	$S_1(n\pi^*)$	3.93	4.85 (4.16)	4.76 (4.71)	
		$S_2(\pi\pi^*)$	6.74	7.19 (6.88)	6.98 (6.87)	
Ura[e]	min S_0	$2^1A_1(n\pi^*)$				4.79
		$3^1A_1(\pi\pi^*)$				5.34
5-CH_3-Ura[e]	min S_0	$2^1A_1(n\pi^*)$				4.82
		$3^1A_1(\pi\pi^*)$				5.20

[a] 6-31G* basis set. [b] MR-CISD calculations with Pople corrections (MR-CISD+Q). The energies without Pople corrections are given in parentheses. [c] Results obtained with the 6-311G(2d,p) basis set are given in parentheses. [d] The results of CC2/SVP vertical excitation energies and values of oscillator strengths (in parentheses) are given in italics. [e] Ref. 66.

showing that the former method provides a reliable description of the PES.

Stationary points of the excited states and minima on the crossing seam. The CASSCF-optimized structures of S_1 ($n\pi^*$) minima for both 5-NH_2-Ura and 5-OH-Ura together with the most important geometrical parameters are given in Fig. 1. For both species, the minima show an elongation of C4–O and C5–C6 bonds and a shortening of the C4–C5 bond with respect to the ground-state geometry. The excited-state minima are also characterized by puckering at the C6 (5-NH_2-Ura) and N3 (5-OH-Ura) atoms and the deviation of the 5-X substituents from planarity. In addition, in the case of 5-OH-Ura, the OH group, which is in the plane of the ring in the ground-state minimum, is significantly rotated out of this plane due to the repulsion of partial positive charges of O(C4) atom caused by the excitation from the lone-pair orbital and H atom of the OH group. The relaxation of the $n\pi^*$ state from the Franck–Condon region (further labeled as 3^1A_1) to the S_1 ($n\pi^*$) minimum leads to lowering of the CASSCF excitation energies by about 1.2 eV and 1.3 eV for 5-NH_2- and 5-OH-Ura, respectively. Using the MR-CISD+Q and MS-CASPT2 methods this lowering amounts to 0.8 and 0.6 eV, respectively. For both species we did not succeed in localizing the minima of $\pi\pi^*$ character at the CASSCF level. Previous studies of uracil and substituted species however indicate that the S_1 global minimum is of $n\pi^*$ character.[25]

The energies, conformational analysis based on the Cremer–Pople parameters,[63] and the character of the wave-function of the minima located on the S_1/S_0 crossing seam for 5-NH_2-Ura and 5-OH-Ura are listed in Tables 2 and 3 respectively; in Fig. 7a and b the corresponding structures are shown.

For both species all structures display strong out-of-plane deformations. Using the Cremer–Pople parameters[63] and the Boeyens classification scheme,[64] we identified four types of structure deformations, namely, boat (B), screw-boat (S), envelope (E), and twist-boat (T) conformations. In most cases the single-point calculations at the MR-CISD and MS-CASPT2 methods using the CASSCF optimized conical

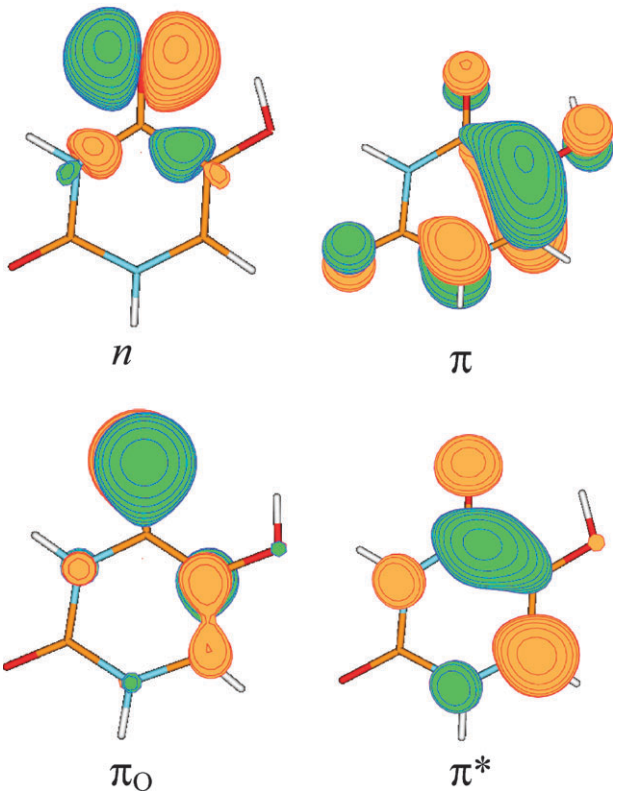

Fig. 5 Molecular orbitals of 5-OH-Ura involved in the $n\pi^*$, $\pi\pi^*$, and $\pi_O\pi^*$excitations. The same character of orbitals was observed for 5-NH_2-Ura.

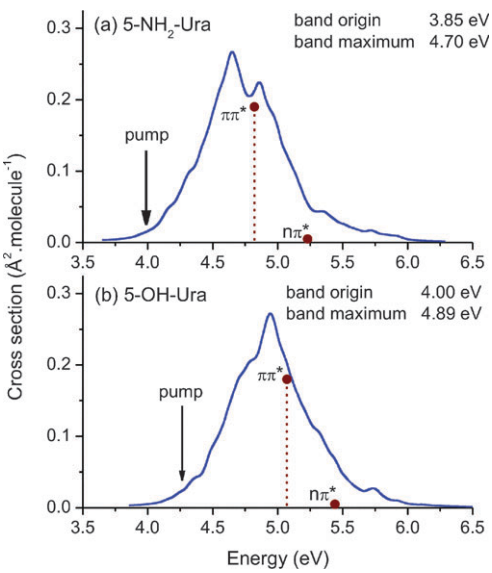

Fig. 6 Absorption spectrum of (a) 5-NH_2-Ura and (b) 5-OH-Ura simulated using the CC2/SVP method. The arrows indicate the region of the spectra pumped in the experiments (see text). The dots show the oscillator strengths and transition energies of the $\pi\pi^*$ and $n\pi^*$ states for the ground-state minimum.

intersection geometries resulted in a S_1/S_0 energy split of up to about 0.8 eV. The reported MR-CISD and CASPT2 energies are taken as the average values of the energies of the S_0 and S_1 states. For an explanation of the excited-state behavior we consider the relative energies of excited-state minima and minima on the crossing seams based on the CASPT2 results.

In the case of 5-NH_2-Ura, based on the results of excitation energies obtained at the MS-CASPT2 level, ^{6}E MXS is the only conical intersection accessible after vertical excitation into the first $\pi\pi^*$ state. This structure is characterized by crossing between the $\pi\pi^*$ and closed shell (cs) surfaces. The singly occupied orbital originates from the π (C5–C6) orbital at the formerly planar structure. Due to the puckering at C6 in the conical intersection structure the orbital becomes localized mainly on this atom. The next E_5 and ^{1,4}B MXSs are already energetically above the bright $2^1A_1(\pi\pi^*)$ state, although the energy gap is only about 0.2 and 0.4 eV, respectively. These structures correspond to $\pi\pi^*$/cs crossings. The other MXS structures are all puckered at the N3 atom and correspond to cs and the $\pi_O\pi^*$ crossings with a contribution from $n\pi^*$. These structures are about 0.7–1.0 eV higher in energy than $2^1A_1(\pi\pi^*)$.

In the case of 5-OH-Ura, the two lowest structures on the S_1/S_0 seam, ^{6}E and $^4S_5$, are characterized by $\pi\pi^*$/cs crossing. Only the former structure is lower in energy than the vertical excitation energy of the $2^1A_1(\pi\pi^*)$ state, while the latter is about 0.4 eV above this state. The character of its wavefunction is the same as in the case of 5-NH_2-Ura. The other higher lying structures are puckered at the N3 atom ($^3T_1$, $^1T_3$, and ^{3}E) and characterized by the crossing between the cs surface with a surface of mainly $\pi_O\pi^*$ character. These structures are about 0.8–1.4 eV above the $2^1A_1(\pi\pi^*)$ state.

Although there is not a unique assignment between the conical intersections of the two uracil analogues the following correspondence of S_1/S_0 MXS structures can be achieved based on the Cremer–Pople parameters, energy ordering and changes due to electron correlation effects: ^{6}E, $^3T_1$, E_5, $B_{3,6}$ and ^{3,6}B structures of 5-NH_2-Ura correspond to ^{6}E, $^3T_1$, $^4S_5$, $^1T_3$ and ^{3}E structures of 5-OH-Ura, respectively. ^{1,4}B of 5-NH_2-Ura does not seem to have a corresponding structure in 5-OH-Ura.

Reaction paths. For both species only the lowest ^{6}E S_1/S_0 conical intersection is expected to be important for nonadiabatic relaxation mechanism, if it occurs after excitation into the first $\pi\pi^*$ state. The other S_1/S_0 conical intersections may be accessed only if higher excited states are populated. The ^{6}E conical intersection can be reached either directly after the excitation into 2^1A_1 or indirectly with the molecule first relaxing to the S_1 minimum of $n\pi^*$ character which was found to be a global minimum for uracil and its substituted analogues.[25] The minimum of the excited state of $\pi\pi^*$ character is expected to occur near its crossing with the ground state after the $n\pi^*/\pi\pi^*$ crossing.[25] Thus the main pathways to internal conversion of the studied species are those which connect the Franck–Condon region or $S_1(n\pi^*)$ minimum with ^{6}E conical intersections as shown in Figs. 8 and 9. These calculations are performed using the MR-CIS/SA-3-CASSCF and CASPT2/SA-5-CASSCF (in its single-state version) methods. For both methods the five lowest states were calculated. In these curves the dashed line indicates the actual state of the molecule along the pathway. Apart from the exchanged order of the $\pi\pi^*$ and $n\pi^*$ states at the ground-state minimum

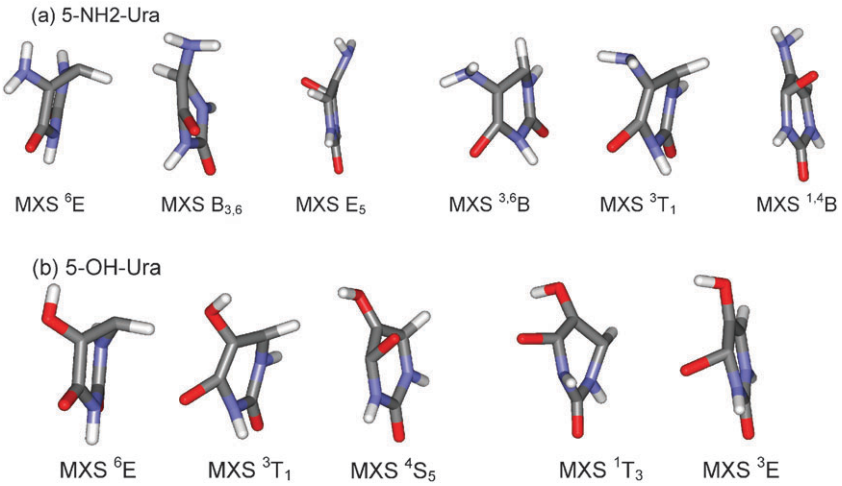

Fig. 7 Geometry of S_1/S_0 MXS for 5-NH_2-Ura (a) and 5-OH-Ura (b).

Table 2 Relative energies in eV of MXS (S_0/S_1) of 5-NH_2-Ura

Geometry	State	CAS(10,8)	MR-CISD[a,b,c]	CASPT2[a,c]
$^{6}E(cs/\pi\pi^*)$	S_0/S_1	4.05	3.73 (3.77)	3.65
	S_2	7.84	7.38 (7.59)	6.95
$B_{3,6}(cs/\pi_O\pi^* + n\pi^*)$	S_0/S_1	5.11	5.93 (5.56)	5.81
	S_2	7.87	8.10 (8.13)	8.05
$E_5(cs/\pi\pi^*)$	S_0/S_1	5.23	5.16 (4.92)	5.01
	S_2	7.50	7.86 (7.42)	7.57
$^{3,6}B(cs/\pi_O\pi^* + n\pi^*)$	S_0/S_1	5.30	5.64 (5.28)	5.55
	S_2	8.33	8.07 (8.06)	8.18
$^{3}T_1(cs/\pi_O\pi^* + n\pi^*)$	S_0/S_1	5.34	5.75 (5.37)	5.69
	S_2	8.40	8.26 (8.19)	8.31
$^{1,4}B(cs/\pi\pi^*)$	S_0/S_1	5.45	5.30 (5.10)	5.20
	S_2	7.08	7.42 (6.98)	7.22

[a] 6-31G* basis set. [b] MR-CISD calculations with Pople corrections (MR-CISD + Q). The energies without Pople corrections are given in parentheses. [c] The average of the S_0 and S_1 state energies is reported.

Table 3 Relative energies in eV of MXS (S_0/S_1) of 5-OH-Ura

Geometry	State	CAS(10,8)	MR-CISD[a,b,c]	CASPT2[a,c]
$^{6}E(cs/\pi\pi^*)$	S_0/S_1	4.66	4.42 (4.40)	4.25
	S_2	8.23	7.76 (7.96)	7.18
$^{3}T_1(cs/\pi_O\pi^* + n\pi^*)$	S_0/S_1	5.35	5.93 (5.45)	5.80
	S_2	8.36	8.49 (8.36)	8.49
$^{4}S_5(cs/\pi\pi^*)$	S_0/S_1	5.31	5.39 (5.44)	5.36
	S_2	7.70	8.50 (8.28)	8.01
$^{1}T_3(cs/\pi_O\pi^* + \pi\pi^*)$	S_0/S_1	5.44	6.28 (5.67)	6.28
	S_2	8.47	9.05 (8.56)	8.95
$^{3}E(cs/\pi_O\pi^*)$	S_0/S_1	5.59	6.16 (5.91)	5.98
	S_2	8.51	8.50 (8.41)	8.17

[a] 6-31G* basis set. [b] MR-CISD calculations with Pople corrections (MR-CISD + Q). The energies without Pople corrections are given in parentheses. [c] The average of the S_0 and S_1 state energies is reported.

discussed above, the MR-CIS and CASPT2 results are in good agreement, displaying the same general reaction pathways.

The interpolated curves which correspond to the reaction paths from the Franck–Condon region towards the conical intersection are described first. For both molecules, the ^{6}E conical intersection is formed by a twist along the C5–C6 bond, which induces the C6 puckering. Along the path towards this conical intersection the $\pi\pi^*$ state changes the character from ionic to biradical.[25] For all naturally occurring pyrimidine nucleobases this pathway has been shown to be barrierless.[65] In the case of 5-substituted uracil, however, the ionic/biradical crossing causes a barrier along the reaction path. This barrier is relatively small at the CASPT2 level (about 0.3 eV) or negligible at the MR-CIS level for 5-NH_2-Ura because of the high energy of the $\pi\pi^*$ state computed at this level. For the more electronegative OH group, the barrier becomes larger, about 0.7 eV at both methods. The same effect of electronegative substituents leading to a barrier was also observed for 5-fluoro-cytosine by Zgierski *et al.*[25] Although the barrier taken from the highest point on the interpolation curve represents only an 'upper-limit' compared to the true barrier, it is high enough to expect its actual existence.

The reaction paths connecting the minima on the $S_1(n\pi^*)$ surface and ^{6}E MXS calculated at the MR-CIS level are characterized by a sizeable barrier of about 1 eV for both species which is a result of the avoided crossing of the state of $n\pi^*$ to $\pi\pi^*$ character at about 4 Å·amu$^{1/2}$. A very similar pathway is obtained by CASPT2 calculations for the 5-OH-Ura molecule. In the case of the 5-NH_2-Ura molecule the barrier along the pathway computed at the CASPT2 level is reduced due to the mixing between the $n\pi^*$ and $\pi\pi^*$ states.

Conclusion

The experimentally determined excited-state lifetimes of two species of 5-X-Ura (X = NH_2 and OH) are significantly different from those observed for uracil (X = H) at 1.5–2.3 ps and thymine (X = CH_3) at 5–6 ps[24,31] upon excitation at 267 nm. That is, however, a higher pump energy, which is not directly comparable to the present experiment, since that energy should excite the system well above any barrier towards internal conversion. We here report data from excitation at the band origin (in the 290–310 nm range) which should excite close to or even below the barrier. Therefore a more relevant comparison is with the work of Brady *et al.* who found a broad UV spectrum with a broad onset at the band origin for uracil

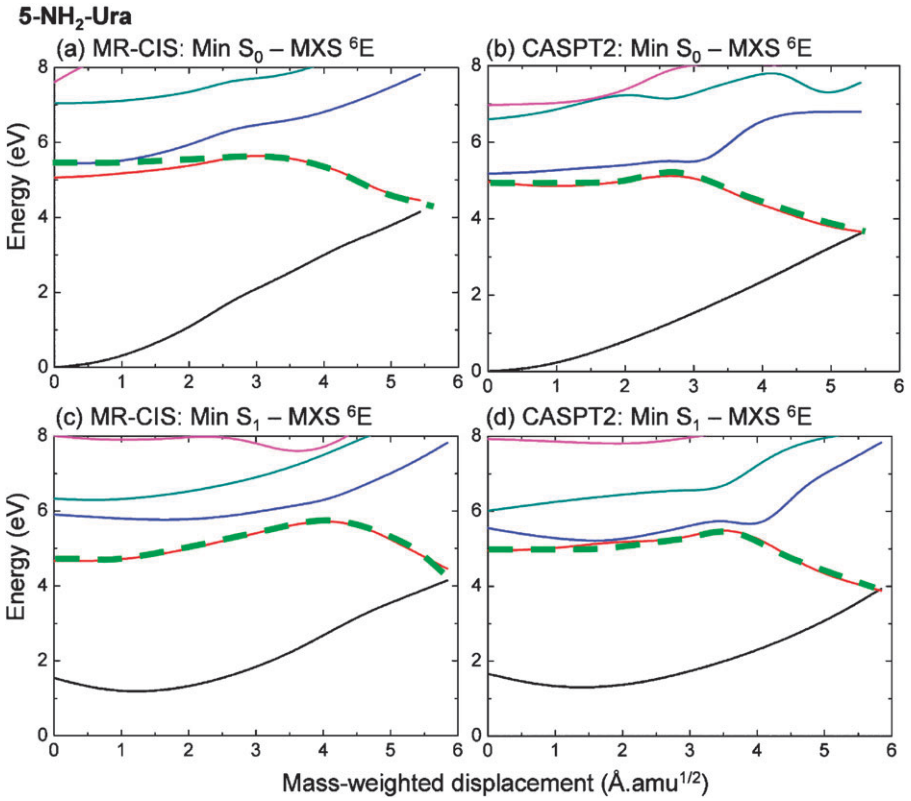

Fig. 8 Potential energy curves for 5-NH_2-Ura: Min S_0 to MXS ^{6}E calculated at the (a) MR-CIS/3-SA-CASSCF and the (b) the CASPT2/5-SA-CASSCF levels. Min S_1 to MXS ^{6}E calculated at the (c) MR-CIS/3-SA-CASSCF and the (d) the CASPT2/5-SA-CASSCF levels. The dashed lines schematically indicate the actual state of the molecule.

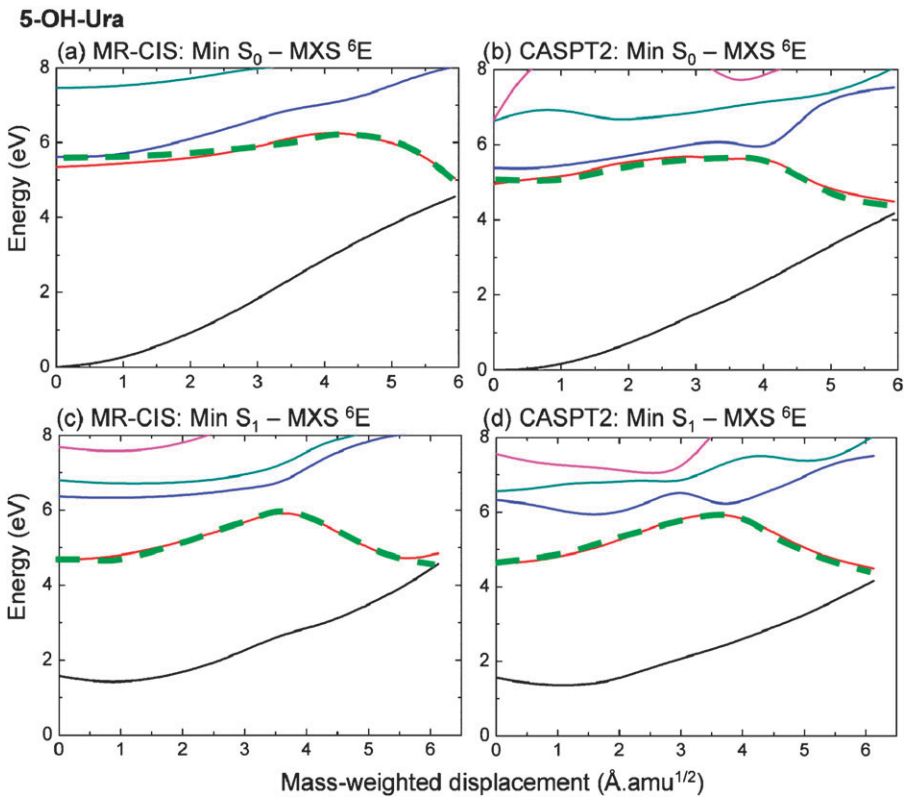

Fig. 9 Potential energy curves for 5-OH-Ura: Min S_0 to MXS ^{6}E calculated at the (a) MR-CIS/3-SA-CASSCF and the (b) the CASPT2/5-SA-CASSCF levels. Min S_1 to MXS ^{6}E calculated at the (c) MR-CIS/3-SA-CASSCF and the (d) the CASPT2/5-SA-CASSCF levels. The dashed lines schematically indicate the actual state of the molecule.

and thymine.[30] That observation suggests a short excited-state lifetime for those two biologically important nucleobases relative to the 1.8 and 12.0 ns lifetimes of the C5-substituted uracils in the comparable energy range.

In order to understand the deactivation mechanisms we computed the most favorable internal conversion pathways through conical intersections. These pathways indicate that the C5-substituted species should relax in excited states differently from thymine and uracil. This difference results from the different ordering of $n\pi^*$ and $\pi\pi^*$ states in the Franck–Condon region and from a different topography of the pathway towards the ethene-like ^{6}E conical intersection, which is the only energetically accessible intersection at the relatively large pump wavelengths used in the experiments. While the path towards this structure is barrierless in the case of natural bases, there is a sizeable barrier for amino- and hydroxyl-substituted species. The barrier height does not simply determine the excited-state lifetime. It determines, however, above what excitation energy the conical intersection becomes accessible: at wavelengths that excite the molecule below the barrier the excited state can be long-lived while at shorter wavelengths that excite the molecule above the barrier the excited state can become very short-lived.

Acknowledgements

This material is based upon work supported by the National Science Foundation under CHE-0911564. This work has been supported by the Austrian Science Fund within the framework of the Special Research Program F16 (Advanced Light Sources) and Project P18411-N19, and by grants from the Ministry of Education of the Czech Republic (Center for Biomolecules and Complex Molecular Systems, LC512). It was part of research project Z40550506. Support from the Preamium Academiae of the Academy of Sciences of the Czech Republic, awarded to PH in 2007, is gratefully acknowledged.

References

1 A. Broo, *J. Phys. Chem. A*, 1998, **102**, 526.
2 E. Nir, K. Kleinermanns, L. Grace and M. S. de Vries, *J. Phys. Chem. A*, 2001, **105**, 5106.
3 K. A. Kistler and S. Matsika, *J. Phys. Chem. A*, 2007, **111**, 2650.
4 E. Mburu and S. Matsika, *J. Phys. Chem. A*, 2008, **112**, 12485.
5 M. Mons, F. Piuzzi, I. Dimicoli, L. Gorb and J. Leszczynski, *J. Phys. Chem. A*, 2006, **110**, 10921.
6 C. M. Marian, *J. Phys. Chem. A*, 2007, **111**, 1545.
7 A. Abo-Riziq, L. Grace, E. Nir, M. Kabelac, P. Hobza and M. S. de Vries, *Proc. Natl. Acad. Sci. U. S. A.*, 2005, **102**, 20.
8 T. Schultz, E. Samoylova, W. Radloff, I. V. Hertel, A. L. Sobolewski and W. Domcke, *Science*, 2004, **306**, 1765.
9 Y. G. He, C. Y. Wu and W. Kong, *J. Phys. Chem. A*, 2004, **108**, 943.
10 K. de La Harpe, C. E. Crespo-Hernandez and B. Kohler, *ChemPhysChem*, 2009, **10**, 1421.
11 A. L. Sobolewski and W. Domcke, *Eur. Phys. J. D*, 2002, **20**, 369.
12 H. R. Hudock, B. G. Levine, A. L. Thompson, H. Satzger, D. Townsend, N. Gador, S. Ullrich, A. Stolow and T. J. Martinez, *J. Phys. Chem. A*, 2007, **111**, 8500.
13 C. M. Marian, M. Kleinschmidt and Tatchen, *Chem. Phys.*, 2008, **347**, 346.
14 G. Zechmann and M. Barbatti, *Int. J. Quantum Chem.*, 2008, **108**, 1266.
15 J. J. Serrano-Pérez, I. Gonzalez-Ramírez, P. B. Coto, M. Merchán and L. Serrano-Andrés, *J. Phys. Chem. B*, 2008, **112**, 14096.
16 Z. G. Lan, E. Fabiano and W. Thiel, *ChemPhysChem*, 2009, **10**, 1225.
17 Z. G. Lan, E. Fabiano and W. Thiel, *J. Phys. Chem. B*, 2009, **113**, 3548.
18 K. Tomić, J. Tatchen and C. M. Marian, *J. Phys. Chem. A*, 2005, **109**, 8410.
19 H. R. Hudock and T. J. Martinez, *ChemPhysChem*, 2008, **9**, 2486.
20 E. Nir, I. Hunig, K. Kleinermanns and M. S. de Vries, *Phys. Chem. Chem. Phys.*, 2003, **5**, 4780.
21 R. J. Malone, A. M. Miller and B. Kohler, *Photochem. Photobiol.*, 2003, **77**, 158.
22 Y. G. He, C. Y. Wu and W. Kong, *J. Phys. Chem. A*, 2003, **107**, 5145.
23 L. Blancafort, B. Cohen, P. M. Hare, B. Kohler and M. A. Robb, *J. Phys. Chem. A*, 2005, **109**, 4431.
24 C. Canuel, M. Mons, F. Piuzzi, B. Tardivel, I. Dimicoli and M. Elhanine, *J. Chem. Phys.*, 2005, **122**, 074316.
25 M. Z. Zgierski, S. Patchkovskii, T. Fujiwara and E. Lim, *J. Phys. Chem. A*, 2005, **109**, 9384.
26 L. Serrano-Andres, M. Merchan and A. C. Borin, *Proc. Natl. Acad. Sci. U. S. A.*, 2006, **103**, 8691.
27 M. Barbatti and H. Lischka, *J. Am. Chem. Soc.*, 2008, **130**, 6831.
28 M. Barbatti and H. Lischka, *J. Phys. Chem. A*, 2007, **111**, 2852.
29 Z. Gengeliczki, M. P. Callahan, N. Svadlenak, C. I. Pongor, B. Sztaray, L. Meerts, D. Nachtigallova, P. Hobza, M. Barbatti, H. Lischka and M. S. de Vries, *Phys. Chem. Chem. Phys.*, 2010, DOI: 10.1039/b917852j.
30 B. B. Brady, L. A. Peteanu and D. H. Levy, *Chem. Phys. Lett.*, 1988, **147**, 538.
31 H. Kang, K. T. Lee, B. Jung, Y. J. Ko and S. K. Kim, *J. Am. Chem. Soc.*, 2002, **124**, 12958.
32 D. C. Lührs, J. Viallon and I. Fischer, *Phys. Chem. Chem. Phys.*, 2001, **3**, 1827.
33 G. Meijer, M. S. Devries, H. E. Hunziker and H. R. Wendt, *Appl. Phys. B: Photophys. Laser Chem.*, 1990, **51**, 395.
34 A. D. Becke, *J. Chem. Phys.*, 1993, **98**, 5648.
35 C. Lee, W. Yang and F. G. Parr, *Phys. Rev. B: Condens. Matter*, 1988, **37**, 785.
36 B. Miehlich, A. Savin, H. Stoll and H. Preuss, *Chem. Phys. Lett.*, 1989, **157**, 200.
37 R. Krishnan, J. S. Binkley, R. Seeger and J. A. Pople, *J. Chem. Phys.*, 1980, **72**, 650.
38 A. D. Mclean and G. S. Chandler, *J. Chem. Phys.*, 1980, **72**, 5639.
39 M. J. Frisch, G. W. Trucks, H. B. Schlegel, G. E. Scuseria, M. A. Robb, J. R. Cheeseman, J. J. A. Montgomery, T. Vreven, K. N. Kudin, J. C. Burant, J. M. Millam, S. S. Iyengar, J. Tomasi, V. Barone, B. Mennucci, M. Cossi, G. Scalmani, N. Rega, G. A. Petersson, H. Nakatsuji, M. Hada, M. Ehara, K. Toyota, R. Fukuda, J. Hasegawa, M. Ishida, T. Nakajima, Y. Honda, O. Kitao, H. Nakai, M. Klene, X. Li, J. E. Knox, H. P. Hratchian, J. B. Cross, V. Bakken, C. Adamo, J. Jaramillo, R. Gomperts, R. E. Stratmann, O. Yazyev, A. J. Austin, R. Cammi, C. Pomelli, J. W. Ochterski, P. Y. Ayala, K. Morokuma, G. A. Voth, P. Salvador, J. J. Dannenberg, V. G. Zakrzewski, S. Dapprich, A. D. Daniels, M. C. Strain, O. Farkas, D. K. Malick, A. D. Rabuck, K. Raghavachari, J. B. Foresman, J. V. Ortiz, Q. Cui, A. G. Baboul, S. Clifford, J. Cioslowski, B. B. Stefanov, G. Liu, A. Liashenko, P. Piskorz, I. Komaromi, R. L. Martin, D. J. Fox, T. Keith, M. A. Al-Laham, C. Y. Peng, A. Nanayakkara, M. Challacombe, P. M. W. Gill, B. Johnson, W. Chen, M. W. Wong, C. Gonzalez and J. A. Pople, *GAUSSIAN 03*, Gaussian, Inc., Wallingford, CT, 2004.
40 R. Shepard, in *Modern Electronic Structure Theory*, ed. D. R. Yarkony, World Scientific, Singapore, 1995, **vol. 1**, pp. 345.
41 R. Shepard, H. Lischka, P. G. Szalay, T. Kovar and M. Ernzehof, *J. Chem. Phys.*, 1992, **96**, 2085.
42 H. Lischka, M. Dallos, P. G. Szalay, D. R. Yarkony and R. Shepard, *J. Chem. Phys.*, 2004, **120**, 7322.
43 H. Lischka, M. Dallos and R. Shepard, *Mol. Phys.*, 2002, **100**, 1647.
44 K. Andersson, P. A. Malmqvist and B. O. Roos, *J. Chem. Phys.*, 1992, **96**, 1218.
45 K. Andersson, P. A. Malmqvist, B. O. Roos, A. J. Sadlej and K. Wolinski, *J. Phys. Chem.*, 1990, **94**, 5483.

46 W. J. Hehre, R. Ditchfield and J. A. Pople, *J. Chem. Phys.*, 1972, **56**, 2256.
47 A. Bunge, *J. Chem. Phys.*, 1970, **53**, 20.
48 S. R. Langhoff and E. R. Davidson, *Int. J. Quantum Chem.*, 1974, **8**, 61.
49 P. J. Bruna, S. D. Peyerimhoff and R. J. Buenker, *Chem. Phys. Lett.*, 1980, **72**, 278.
50 G. Ghigo, B. O. Roos and P. A. Malmqvist, *Chem. Phys. Lett.*, 2004, **396**, 142.
51 O. Christiansen, H. Koch and P. Jorgensen, *Chem. Phys. Lett.*, 1995, **243**, 409.
52 C. Hättig and F. Weigend, *J. Chem. Phys.*, 2000, **113**, 5154.
53 C. Hättig and A. Köhn, *J. Chem. Phys.*, 2002, **117**, 6939.
54 (*a*) A. Schäfer, C. Huber and R. Ahlrichs, *J. Chem. Phys.*, 1994, **100**, 5829; (*b*) A. Schäfer, H. Horn and R. Ahlrichs, *J. Chem. Phys.*, 1992, **97**, 2571.
55 J. P. Bergsma, P. H. Berens, K. R. Wilson, D. R. Fredkin and E. J. Heller, *J. Phys. Chem.*, 1984, **88**, 612.
56 H. Lischka, R. Shepard, R. M. Pitzer, I. Shavitt, M. Dallos, T. Muller, P. G. Szalay, M. Seth, G. S. Kedziora, S. Yabushita and Z. Y. Zhang, *Phys. Chem. Chem. Phys.*, 2001, **3**, 664.
57 H. Lischka, R. Shepard, F. B. Brown and I. Shavitt, *Int. J. Quant. Chem.*, 1981, **20**, 91.
58 H. Lischka, R. Shepard, I. Shavitt, R. M. Pitzer, T. Muller, P. G. Szalay, S. R. Brozell, G. Kedziora, E. A. Stahlberg, R. J. Harrison, J. Nieplocha, M. Minkoff, M. Barbatti, M. Schuurmann, D. R. Yarkony, S. Matsika, E. V. Beck and J.-P. Blaudeau, COLUMBUS, an ab initio electronic structure program; release 5.9.1, 2006, www.univie.ac.at/columbus.
59 G. Karlstrom, R. Lindh, P. A. Malmqvist, B. O. Roos, U. Ryde, V. Veryazov, P. O. Widmark, M. Cossi, B. Schimmelpfennig, P. Neograd y and L. Seijo, *Comput. Mater. Sci.*, 2003, **28**, 222.
60 R. Ahlrichs, M. Bar, M. Haser, H. Horn and C. Kolmel, *Chem. Phys. Lett.*, 1989, **162**, 165.
61 M. Barbatti, G. Granucci, M. Persico, M. Ruckenbauer, M. Vazdar, M. Eckert-Maksic and H. Lischka, *J. Photochem. Photobiol., A*, 2007, **190**, 228.
62 M. Barbatti, G. Granucci, M. Ruckenbauer, J. Pittner, M. Persico and H. Lischka, *NEWTON-X: a package for Newtonian dynamics close to the crossing seam*, 2007, www.univie.ac.at/newtonx.
63 D. Cremer and J. A. Pople, *J. Am. Chem. Soc.*, 1975, **97**, 1354.
64 J. C. A. Boeyens, *J. Chem. Crystallogr.*, 1978, **8**, 317.
65 M. Merchán, R. González-Luque, T. Climent, L. Serrano-Andrés, E. Rodríguez, M. Reguero and D. Peláez, *J. Phys. Chem. B*, 2006, **110**, 26471.
66 T. Fleig, S. Knecht and C. Hättig, *J. Phys. Chem. A*, 2007, **111**, 5482.